



HAL
open science

On a wave-based reduced order model for transient effects computation including mid frequencies

Philippe de Brabander, Olivier Allix, Pierre Ladèveze, Pascal Hubert, Pascal Thevenet

► **To cite this version:**

Philippe de Brabander, Olivier Allix, Pierre Ladèveze, Pascal Hubert, Pascal Thevenet. On a wave-based reduced order model for transient effects computation including mid frequencies. *Computer Methods in Applied Mechanics and Engineering*, 2022, 395, pp.114990. 10.1016/j.cma.2022.114990 . hal-03926553

HAL Id: hal-03926553

<https://hal.science/hal-03926553>

Submitted on 22 Jul 2024

HAL is a multi-disciplinary open access archive for the deposit and dissemination of scientific research documents, whether they are published or not. The documents may come from teaching and research institutions in France or abroad, or from public or private research centers.

L'archive ouverte pluridisciplinaire **HAL**, est destinée au dépôt et à la diffusion de documents scientifiques de niveau recherche, publiés ou non, émanant des établissements d'enseignement et de recherche français ou étrangers, des laboratoires publics ou privés.



Distributed under a Creative Commons Attribution - NonCommercial 4.0 International License



ELSEVIER

Available online at www.sciencedirect.com**ScienceDirect**

Comput. Methods Appl. Mech. Engrg. 395 (2022) 114990

**Computer methods
in applied
mechanics and
engineering**www.elsevier.com/locate/cma

On a wave-based reduced order model for transient effects computation including mid frequencies

Philippe De Brabander^a, Olivier Allix^{a,*}, Pierre Ladèveze^a, Pascal Hubert^b,
Pascal Thevenet^b

^a *Université Paris-Saclay, ENS Paris-Saclay, CentraleSupélec, LMPS - Laboratoire de Mécanique Paris-Saclay, 4 Avenue des Sciences, 91190 Gif-sur-Yvette, France*

^b *ArianeGroup, 66 Route de Verneuil, 78130 Les Mureaux, France*

Received 5 March 2021; received in revised form 4 April 2022; accepted 9 April 2022

Available online xxx

Abstract

The wave-based computational method named Variational Theory of Complex Rays (VTCR) is revisited in order to improve its robustness and its efficiency to solve transient dynamic problems including medium frequencies. The first problem addressed in the paper concerns the ill-conditioning of wave-based computational approaches. We introduce the concept of “effective portrait” which provides a new framework to the VTCR with a strong reduction of the conditioning number. The second issue deals with the computation over a large frequency bandwidth for which the Proper Generalised Decomposition (PGD) has been retained. A thorough analysis of the efficiency and the limitations of the PGD-VTCR is given. The last issue concerns the synergy between the PGD-VTCR and the exponential window method for solving transient problems.

© 2022 Elsevier B.V. All rights reserved.

Keywords: VTCR; Model reduction; PGD; Dynamic transient response; Exponential window method

1. Introduction

Simulation of dynamic structural response is an important part of industrial design. Numerical methods were designed to deal with the transient response but they remain ineffective when medium frequencies should be taken into account to properly describe the energetic response. This is the case of the simulation of pyrotechnic shocks which motivates this work. In dynamics the Finite Element Method (FEM) [1] associated with time integration is, by far, the most widely used approach. FEM allows the low frequency range to be easily processed. Reduced basis with vibration modes are also very used. Processing higher frequencies involves a significant refinement of the spatial and temporal meshes. This is mainly due to the pollution error [2]. This error increases as $(\frac{h}{q\lambda})^{2q}$, where h is the size of the element, λ the wavelength and q the degree of interpolation. To preserve accuracy, h should decrease accordingly to the wavelength. This increases the computational cost drastically in the case of medium and high frequencies.

* Corresponding author.

E-mail address: olivier.allix@ens-paris-saclay.fr (O. Allix).

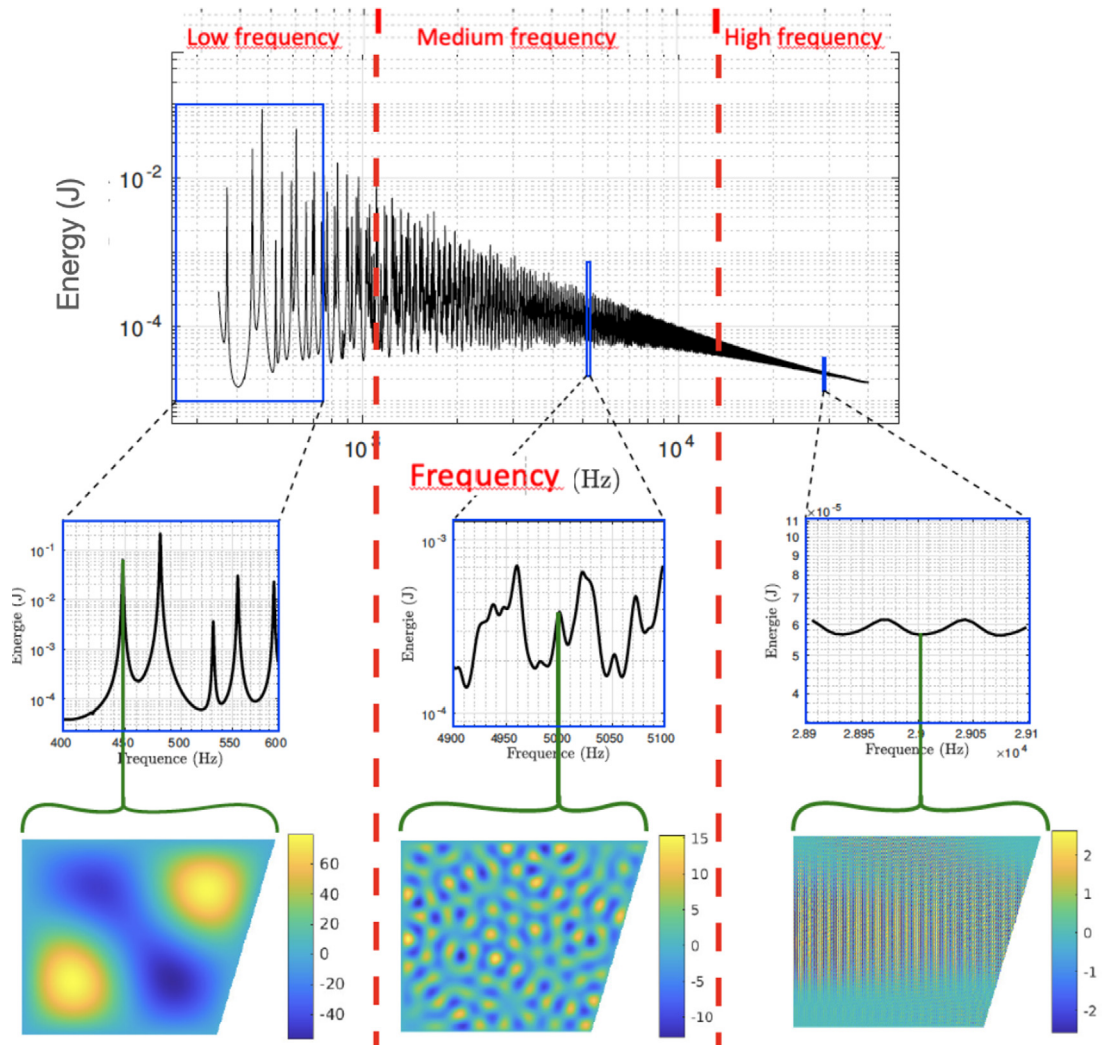


Fig. 1. Frequency spectrum associated with the acoustic response of a cavity to a short impulse (computed with the approach developed in this paper).

The definition of what is low, medium or high frequency is merely qualitative. Fig. 1 illustrates the conventional presentation of the different frequency domains based on the peak overlap due to damping. For us, the medium frequency range is more a region for which the conventional FE computational approach starts to not work well. To deal with transient or vibration responses involving medium or high frequencies, a first set of enhancements FEM approaches have been proposed. Among them one can cite: higher-order methods [3], Galerkin least squares method [4], predefined reduced bases [5], the Partition of Unity Method (PUM) [6], the generalised finite element method [7] and the Discontinuous Petrov Galerkin method [8]. Another set of quite different methods are wave-based methods working on the frequency-space domain originally designed for medium frequency forced vibration problems. They are particular Trefftz methods using shape functions verifying the inner equations at a given frequency. They allow to drastically reduce the number of shape functions. In fact, for a given accuracy they present a weak dependence to the wavelength. One of this method is the Variational Theory of Complex Rays (VTCR) [9] studied in this paper. Others Trefftz methods have been proposed in the literature. Among them the Wave Based Method [10], the Discontinuous Enrichment Method [11], the Wave Boundary Element Method [12]. A survey of

these methods can be found in [13] and in [14]. Compared to usual FEM approaches, their efficiencies have been clearly demonstrated.

Wave-based methods are today mature. For example, the VTCR has been applied to 3D plate assemblies [15], to shell structures [16], and to acoustic problems [17]. First applications to transient dynamics involving medium frequencies has been done in [18] for 3D plate assemblies and in [19] for civil engineering structures.

The objective of this paper is to improve the robustness and the efficiency of the VTCR. The goal is to enable with the VTCR large bandwidth reduced modelling approaches in order to computing transient response involving medium frequencies. For the sake of simplicity, only acoustic problems are considered.

For this, a fundamental question is re-analysed in this paper. It concerns the ill-conditioning of wave-based methods due to the presence in the solution of zero-energy modes. This has a very small impact on the true solution (displacement, pressure, energy) but not on the VTCR solution called “portrait” which is quite erratic. First answers to reduce the conditioning number have been given in [20,21]. Here, we introduced a simpler way with the concept of “effective portrait” which is no more erratic; zero-energy modes are eliminated thanks to a SVD.

The second aspect of the paper concerns large frequency band computational techniques. Such approaches are which is useful for both vibration and transient problems. Several techniques have been already introduced as Padé approximants [22,23]. [19], frequency-polynomial approximation [18], Proper Generalised Decomposition with frequency/space separation [24]. Here, the PGD in the new VTCR framework involving “effective portraits” is revisited. A thorough analysis of this new PGD version is given in terms of damping and bandwidths. It shows the interest but also the limits of this technique when the damping is low.

Based on this last remark the VTCR-PGD approach is coupled to the exponential window approach (EMW) introduced in Ref. [25]. The interest of the EMW here is to allow the damping to be artificially increased. A basic example is used to define the range of parameters that are appropriated for the EMW in the context of the paper. Finally, the PGD-VTCR coupled to the EMW is applied to a shock propagation in an acoustic cavity over a long period of time. This allows illustrating the interest and potentialities of this technique and proposing perspectives for further researches.

2. The acoustic reference problem

In a preamble, let us recall that we are interested in solving the mid-frequency response of the problem. In this band with a high modal density the question of damping is crucial. The damping is often modelled through information coming from experiments in the frequency domain. Those models, as for the hysteretic model of damping, do not have a counterpart in the time domain. Nevertheless, the description of the problem in the frequency domain is probably easier to understand starting from the one in the time domain. Then the model of damping is adapted to incorporate the information relating the wave number and the frequency. This is the approach we follow hereafter.

2.1. The reference problem in the time domain

Let us consider the general 2D interior dynamics problem of a bounded acoustic domain Ω , filled with a fluid characterised by celerity c , density ρ and a viscosity μ . The boundary $\partial\Omega$ is divided into three parts: $\partial_p\Omega$ where the pressure p_d is imposed, $\partial_v\Omega$ where the velocity is imposed v_d and $\partial_h\Omega$ the mixed loading h_d is imposed. The problem is studied over a time interval $I_t = [0, T]$. The initial conditions are considered to be zero. The problem to be solved is: find the pressure field p such:

$$\left\{ \begin{array}{l} \Delta p + \mu \Delta \frac{\partial p}{\partial t} - \frac{1}{c^2} \frac{\partial^2 p}{\partial t^2} = 0 \quad \text{in } \Omega \times I_t \\ \frac{\partial p}{\partial t} + \frac{z}{\rho} \frac{\partial p}{\partial \mathbf{n}} = \frac{\partial h_d}{\partial t} \quad \text{over } \partial_h \Omega \times I_t \\ p = p_d \quad \text{over } \partial_d \Omega \times I_t \\ -\frac{\partial p}{\partial \mathbf{n}} = \rho \frac{\partial v_d}{\partial t} \quad \text{over } \partial_v \Omega \times I_t \end{array} \right. \quad (1)$$

where Δ is the Laplacian operator, \mathbf{n} is the outward normal to $\partial\Omega$ and z the impedance coefficient.

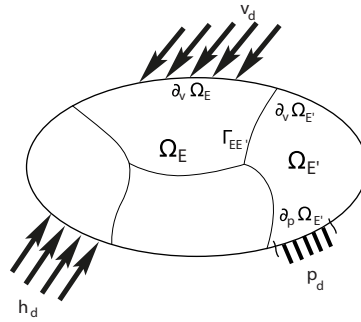


Fig. 2. A general 2D bounded acoustic problem.

2.2. The reference problem in the frequency domain

The treatment of the reference problem in the frequency domain will concern only the mid-frequency range. The low-frequency one is assumed to be treated in the time domain. The criterion splitting the frequencies into low and mid-frequency domains is discussed in [26].

We therefore consider that $\{H_d, P_d, V_d, V_d\}$ are not null only for $\omega \in I_\omega = [\omega_0 - \frac{\Delta\omega}{2}, \omega_0 + \frac{\Delta\omega}{2}]$. The acoustic problem (1) is written in the frequency domain by making use of the Fourier Transform (FT):

$$P(\omega) = FT(p)(\omega) = \int_{t=0}^{+\infty} p(t)e^{i\omega t} dt \tag{2}$$

Denoting $k^2 = \frac{\omega^2}{c^2(1+i\omega\mu)}$, the reference problem can be reformulated as to find the pressure field P such that:

$$\left\{ \begin{array}{l} \Delta P + k^2 P = 0 \quad \text{in } \Omega \times I_\omega \\ P - Z \frac{i}{\omega\rho} \frac{\partial P}{\partial \mathbf{n}} = H_d \quad \text{over } \partial_h \Omega \times I_\omega \\ P = P_d \quad \text{over } \partial_d \Omega \times I_\omega \\ -\frac{\partial P}{\partial \mathbf{n}} = i\omega\rho V_d \quad \text{over } \partial_v \Omega \times I_\omega \end{array} \right. \tag{3}$$

In the paper the following description of the damping is chosen:

$$k = \frac{\omega}{c}(1 - i\eta), \tag{4}$$

where the damping coefficient η is small and assumed to be constant. To rebuild the time response, the inverse of the Fourier Transform is used:

$$p(t) = FT^{-1}(P)(t) = \frac{1}{2\pi} \int_{\omega=-\infty}^{\infty} P(\omega)e^{-i\omega t} d\omega \tag{5}$$

Numerically, the problem is treated for a discrete number of frequencies and the Discrete Fourier Transform (DFT) and Inverse Discrete Fourier Transform (IDFT) are used. When FT is used to construct the time response from a frequency resolution, there may be an error called time overlap (see [25]). This occurs when the signal is not damped at the end of the time interval. To deal with this problem, the frequency step is defined by $\delta\omega = \frac{2\pi}{T_d}$ with T_d the time required to damp the signal. Thereafter, we will denote the corresponding N_ω frequencies as follows:

$$I_\omega = \{\omega_0 - \frac{\Delta\omega}{2}, \omega_0 - \frac{\Delta\omega}{2} + \delta\omega, \dots, \omega_0 + \frac{\Delta\omega}{2}\}.$$

3. Resolution of the acoustic problems frequency by frequency using the VTCR

3.1. The variational formulation

Let us consider a partition of Ω into N_Ω non overlapping sub-cavities (Fig. 2), called VTCR elements. In order to simplify, the following notations are used in the paper:

- Ω_E is the generic name used in what follows for the subcavity E .
- $\Gamma_{E,E'}$ denotes the common interfaces between subcavity E and E' .

With these notations, the reference problem (3) becomes, in the sub-structured version, find, in each sub-structure E , the pressure field P_E such that:

$$\left\{ \begin{array}{l} \Delta P_E + k^2 P_E = 0 \quad \text{in } \Omega_E \times I_\omega \\ P_E - Z \frac{i}{\rho \omega} \frac{\partial P_E}{\partial \mathbf{n}_E} = H_d \quad \text{over } \partial_h \Omega_E \times I_\omega \\ P_E = P_d \quad \text{over } \partial_p \Omega_E \times I_\omega \\ - \frac{\partial P}{\partial \mathbf{n}_E} = i \omega \rho V_d \quad \text{over } \partial_v \Omega_E \times I_\omega \\ P_E = P_{E'} \quad \text{over } \Gamma_{E,E'} \times I_\omega \\ \frac{\partial P_E}{\partial \mathbf{n}_E} = - \frac{\partial P_{E'}}{\partial \mathbf{n}_{E'}} \quad \text{over } \Gamma_{E,E'} \times I_\omega \end{array} \right. \quad (6)$$

The two last equations correspond to the pressure and velocity continuity equations between the different sub-cavities.

Let us introduce the space \mathcal{S}_E of pressure fields that satisfy the homogeneous acoustic equation:

$$\mathcal{S}_E = \{ P_E / \Delta P_E + k^2 P_E = 0 \quad \forall \mathbf{x} \in \Omega_E \times I_\omega \} \quad (7)$$

The following energetic norm will be used throughout the paper:

$$\| P_E \|_{\mathcal{S}_E}^2 = \frac{1}{2 \rho c^2} \int_{\Omega_E} \frac{1}{|k|^2} |\nabla P_E|^2 + |P_E|^2 d\Omega \quad (8)$$

The VTCR verify the border equations through a variational formulation. The VTCR formulation of the problem (6) leads to find in each substructure E the pressure field P_E such that $\forall Q_E \in \mathcal{S}_E$:

$$\begin{aligned} & \sum_{E=1}^{N_E} \frac{1}{2} \int_{\partial_h \Omega_E} \left(P_E - \frac{iZ}{\omega \rho} \frac{\partial P_E}{\partial \mathbf{n}_E} - H_{dE} \right) \left(\frac{\omega \rho}{iZ} Q_E^* - \frac{\partial Q_E^*}{\partial \mathbf{n}_E} \right) d\partial\Omega \\ & + \sum_{E=1}^{N_E} \int_{\partial_p \Omega_E} (P_E - P_{dE}) \frac{\partial Q_E^*}{\partial \mathbf{n}_E} d\partial\Omega + \sum_{\Omega_E} \int_{\partial_v \Omega_E} \left(\frac{\partial P_E}{\partial \mathbf{n}_E} + i \omega \rho V_{dE} \right) Q_E^* d\partial\Omega + \\ & + \sum_{E,E' < E} \frac{1}{2} \int_{\Gamma_{E,E'}} \left[(P_E - P_{E'}) \left(\frac{\partial Q_E^*}{\partial \mathbf{n}_E} - \frac{\partial Q_{E'}^*}{\partial \mathbf{n}_{E'}} \right) + \right. \\ & \quad \left. \left(\frac{\partial P_E}{\partial \mathbf{n}_E} + \frac{\partial P_{E'}}{\partial \mathbf{n}_{E'}} \right) (Q_E^* + Q_{E'}^*) \right] dS = 0 \end{aligned} \quad (9)$$

where the symbol $*$ is used to designate the imaginary conjugate quantity. In [20], this formulation was shown to be equivalent to the reference problem, provided there is damping.

3.2. Approximation spaces and associated problem to be solved

In the VTCR the unknowns, per subdomain, are the *amplitude distribution* $a_E(\theta)$. Several discretisations strategies for the amplitude have been proposed for VTCR: continuous piece-wise functions, truncated Fourier series [27] and Dirac distributions. This last approach is adopted because it facilitates the integration of the variational formulation (9). In fact the integration is then analytical for straight borders [16]. The amplitude distribution is thus expressed as follows:

$$a_E(\theta) = \sum_{n=1}^{N_E} A_n^E \delta_{\theta_n}(\theta) \quad (10)$$

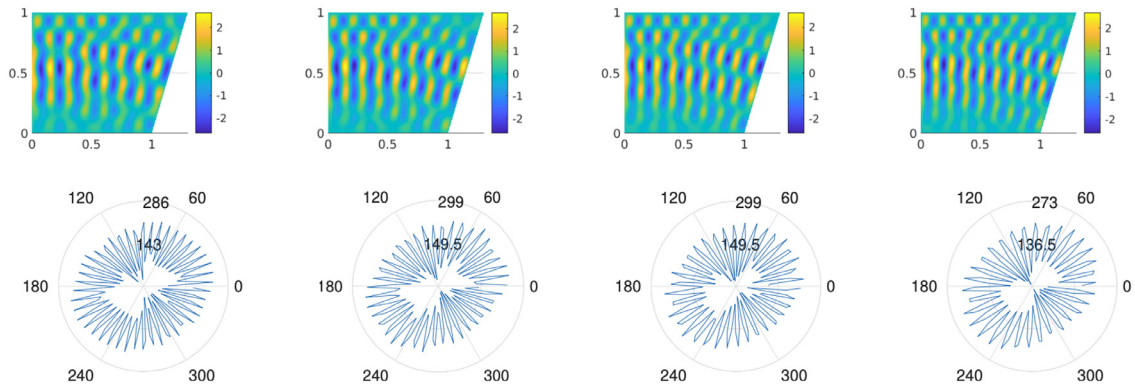


Fig. 3. VT CR resolution of a quadrilateral cavity, $\eta = 10^{-2}$, (from up to down): pressure field, amplitude distribution (in Pa), for different frequencies (from left to right): 2300 Hz, 2433 Hz, 2567 Hz and 2700 Hz.

leading to a plane wave approximation for the pressure field:

$$p_E = \sum_{i=1}^{N_E} A_{E,i}^E e^{ikn(\theta_i) \cdot (x-x_E)} \tag{11}$$

where $A_{E,i}$ is the complex plane wave amplitude, the vector A_E being called the amplitude portrait for the element E .

The injection of these shape functions into the Galerkin variational formulation leads to the following set of linear systems to be solved at each frequency ω :

$$K(\omega)(\omega)A = F(\omega) \tag{12}$$

with A the unknown amplitude vector, K the squared matrix operator, and F the right hand side vector. Moreover,

$$K = \begin{pmatrix} \vdots & & \\ \dots & K_{EE'} & \dots \\ \vdots & & \end{pmatrix} \tag{13}$$

where $K_{EE'}$ is the block corresponding to the coupling between element E and E' .

4. The concept of effective amplitude portrait

4.1. Description of the difficulties

Ill-conditioning of Trefftz formulations, such as the VT CR, is well-known. Its impact on the true solution, here the pressure, is weak excepted for large scale problems. On the contrary, its impact is very important on the amplitude portrait which is erratic. This is because the amplitude portrait takes into account nearly zero energy modes. This phenomenon, which can be seen in Fig. 3, is a serious drawback for all model reduction method based on the portrait.

The goal of the effective portrait is to eliminate, a priori, the nearly zero-energy mode.

4.2. Relation between the portrait and the energy: energy matrix

Let us consider the element E and a N_E uniform discretisation of $[0, 2\pi]$ with $\Delta\theta = \frac{2\pi}{N_E}$. The starting point to construct the effective amplitude portrait is to consider the energy over the element E . From Eq. (11), one obtains

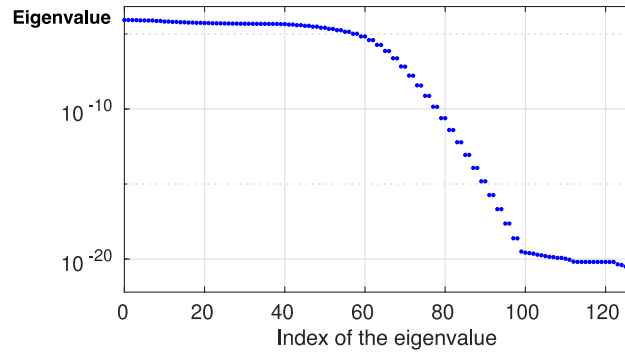


Fig. 4. Eigenvalues in terms of the index for a rectangular cavity.

the following expression which is proportional to the energy:

$$\int_{\Omega_E} |p_E|^2 d\Omega_E = \int_{\Omega_E} \sum_{i=1}^{N_E} \sum_{j=1}^{N_E} A_{E,j}^* A_{E,i} e^{i(k\mathbf{n}(\theta_i) - k^* \mathbf{n}(\theta_j)) \cdot (\mathbf{x} - \mathbf{x}_E)} d\Omega_E \tag{14}$$

$$= \sum_{i=1}^{N_E} \sum_{j=1}^{N_E} A_{E,j}^* A_{E,i} (M_E)_{ji} = A_E^{*T} M_E A_E$$

where M_E is a $N_E \times N_E$ real, symmetric and positive matrix.

Let us consider the typical case of a rectangular domain ($2H_1 \times 2H_2$) in the case of interest where η is small. The expression of the coefficient of the matrix M_E is the following:

$$(M_E)_{ij} = H_1 H_2 \frac{\exp(\alpha_{ij} H_1) - \exp(-\alpha_{ij} H_1)}{\alpha_{ij} H_1} \frac{\exp(\beta_{ij} H_2) - \exp(-\beta_{ij} H_2)}{\beta_{ij} H_2} \tag{15}$$

with:

$$i(k\mathbf{n}(\theta_i) - k^* \mathbf{n}(\theta_j)) = \alpha_{ij} \mathbf{n}(0) + \beta_{ij} \mathbf{n}\left(\frac{\pi}{2}\right) \tag{16}$$

The eigenvalues of the Matrix M_E have been computed for a rectangular cavity ($c = 340 \text{ m s}^{-1}$, $\rho = 1.3 \text{ kg m}^{-2}$, $\eta = 10^{-4}$, $H_1 = 0.5 \text{ m}$, $H_2 = 0,85 \text{ m}$) using $N_E = 126$. One can notice a rather large plateau of eigenvalues corresponding to more or less the same energy and, after, an exponential decrease of the eigenvalues corresponding nearly zero-value energy modes Fig. 4). The later being excited in the classical portrait. This situation is typical of the subdomains used in practice (see .

4.3. Effective portrait definition and fundamental associated properties

To analyse the fundamental properties of the effective portrait and its relation to the energy, it is interesting to consider the continuous case. The continuous formulation can be defined as:

$$p_E = \int_0^{2\pi} A_{E,\theta} e^{ik\mathbf{n}(\theta) \cdot (\mathbf{x} - \mathbf{x}_E)} d\theta \tag{17}$$

Thus:

$$\int_{\Omega_E} |p_E|^2 d\Omega_E = \int_0^{2\pi} d\theta \int_0^{2\pi} d\theta' A_{E,\theta'}^* A_{E,\theta} z(\theta, \theta') \tag{18}$$

with:

$$z(\theta, \theta') = \int_{\Omega_E} e^{i(k\mathbf{n}(\theta) - k^* \mathbf{n}(\theta')) \cdot (\mathbf{x} - \mathbf{x}_E)} d\Omega_E \tag{19}$$

Therefore:

$$(M_E)_{ij} = z(\theta_i, \theta_j) \tag{20}$$

The effective portrait is defined from the eigenmodes of the following eigenvalue problem, find $(\tilde{\lambda}, \tilde{A}_{E\theta})$ such that:

$$\int_0^{2\pi} d\theta' z(\theta, \theta') \tilde{A}_{E\theta} = \tilde{\lambda} \tilde{A}_{E\theta}; \quad \theta \in [0, 2\pi] \tag{21}$$

The eigenmodes $\tilde{A}_{E\theta}^i$ being chosen such that:

$$\int_0^{2\pi} d\theta \int_0^{2\pi} d\theta' \tilde{A}_{E\theta'}^{i*} z(\theta, \theta') \tilde{A}_{E\theta}^i = 1 \tag{22}$$

For a circular domain the eigen modes $\tilde{A}_{E\theta}^i$ are equal to $e^{ir\theta}$. The effective portrait is then defined as a combination of the eigenmodes:

$$A_\theta^{eff} = \sum_{i=1}^{+\infty} a_i \tilde{A}_{E\theta}^i \tag{23}$$

the a_i being such that:

$$p_E = \int_0^{2\pi} e^{ikn(\theta) \cdot (x - x_E)} A_\theta^{eff} d\theta \tag{24}$$

and one has:

$$\int_{\Omega_E} |p_E|^2 d\Omega_E = \|A^{eff}\|^2 = 2\pi \sum_{i=1}^{+\infty} \int_0^{2\pi} |a_i|^2 \tag{25}$$

It follows the fundamental property that p small leads to $\|A^{eff}\|$ small and reciprocally. Thus the effective portrait is not polluted by nearly zero energy-modes.

4.4. On the use of the effective portrait and comparison with the original portrait

The use of the effective portrait implies the computation of the first eigen-modes $\tilde{A}_{E\theta}^i$ for each element. This computation can be done off line and does not imply large computational costs because the number of VTCR elements is usually not large.

In order to illustrate the property of the effective portrait and compare it to the original one a simple example is used. One considers an acoustic cavity with a celerity $c = 340 \text{ m s}^{-1}$ subjected to a pressure $p(x) = \frac{1 - \cos(2\pi x)}{2}$ on the left edge, where x is the curvilinear abscissa. Zero Dirichlet boundary is applied on the other edges.

The solution is built with 1 VTCR element and 127 rays for 4 frequencies: $f = [2300, 2433, 2567, 2700]$ Hz. The pressure field, the original *amplitude distribution* and the *effective* one are reported in Figs. 5 and 6 for two levels of damping. The standard amplitude portrait presents strong oscillations characteristic of the presence of nearly zero energy mode. On the contrary the effective portrait reflects the privileged directions of the pressure field. One can also remark the great influence of the damping. Let us note that the two different amplitude distributions have not the same unit, one is expressed in Pa and the other in $\text{J}^{1/2}$. For the comparison the *amplitude distribution* should and has be multiplied by a scalar depending on the domain: $\frac{V(\Omega_E)}{\sqrt{2\rho c}}$, with $V(\Omega_E)$ the surface of the 2D Ω_E sub-domain.

An interesting feature of the effective portrait is that it allows visualising the direction and intensity of the propagation of energy which ensures the dynamic equilibrium at a given frequency. The example of presented Fig. 7 corresponds to a 2D analysis of a car at a high frequency equal to 10 kHz.

5. A posteriori reduction using the SVD of the solution over a frequency band

The objective here is to study whether it is possible or not to approximate the solution using a low rank approximation over a frequency band. Let us consider frequency dependency on of the VTCR pressure solution (11). It is sought as a two-scale description. In fact, the effective amplitude is expected to be a slow varying term

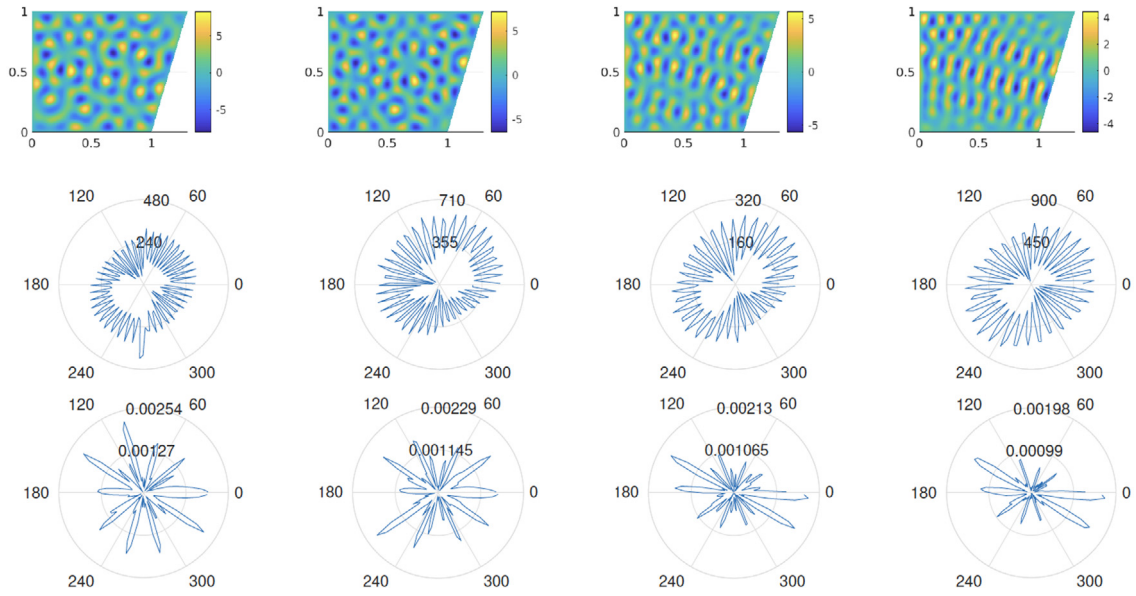


Fig. 5. VTCR resolution of a quadrilateral cavity, $\eta = 10^{-3}$, (from up to down): pressure field, classic *amplitude distribution* (expressed in Pa), and *effective amplitude distribution* (expressed in $J^{1/2}$) for different frequencies (from left to right): 2300 Hz, 2433 Hz, 2567 Hz and 2700 Hz.

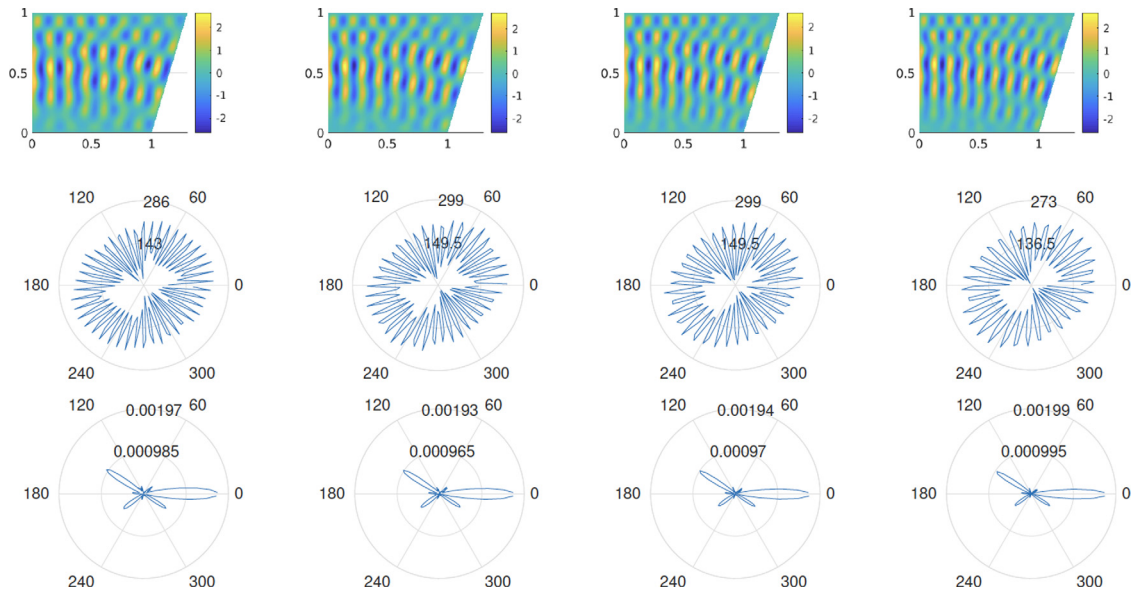


Fig. 6. VTCR resolution of a quadrilateral cavity, $\eta = 10^{-2}$, (from up to down): pressure field, classic *amplitude distribution* (expressed in Pa), and *effective amplitude distribution* (expressed in $J^{1/2}$) for different frequencies (from left to right): 2300 Hz, 2433 Hz, 2567 Hz and 2700 Hz.

with respect to the exponential which is a rapid varying term in mid-frequency. This is why a reduced solution is sought in terms of the effective amplitude distribution only. In each VTCR element E , the later distribution is searched as:

$$a_E^{M-ef}(\omega) = \sum_{m=1}^M A_{E-m}^{eff} \lambda_{E-m}^{eff}(\omega) \tag{26}$$

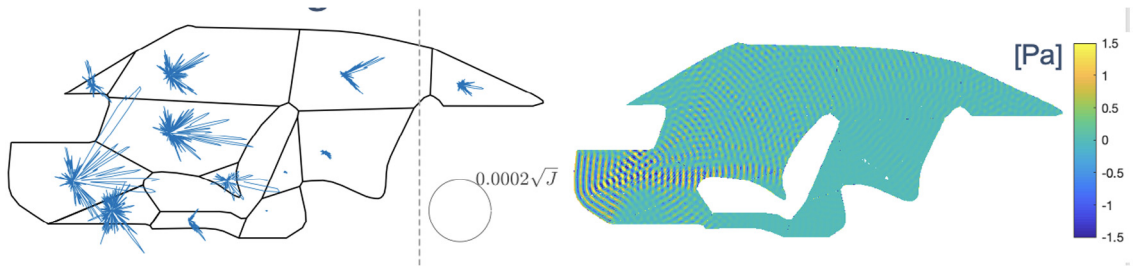


Fig. 7. VTCR resolution and effective portrait for a 2D model of the interior of a car for a frequency of 10 kHz.

where A_m is a vector which contains the portrait of all the elements. The associated modulation $\lambda_m(\omega)$ is a scalar function. The question is to see whether the pressure field may be approximate over the frequency range I_ω by means of a few modes M of the effective amplitude distribution.

The pressure field computed frequency per frequency is taken as a reference. The problem to be solved is to find the different modes that minimise the following quantity:

$$\int_{I_\omega} \|p_{ref} - p_E^M\|_{S_E}^2 d\omega \tag{27}$$

Thanks to the relation (25) this minimisation may be performed, whatever M , using a Singular Value Decomposition (SVD) of the following matrix:

$$\mathbb{A}_{E\ ef} = \begin{pmatrix} A_{E\ ef}(\theta_1, \omega_1) & \dots & A_{E\ ef}(\theta_1, \omega_{N_\omega}) \\ \vdots & & \vdots \\ A_{E\ ef}(\theta_{N_\theta}, \omega_1) & \dots & A_{E\ ef}(\theta_{N_\theta}, \omega_{N_\omega}) \end{pmatrix} \tag{28}$$

The result provides, for $\mathbb{A}_{E\ ef}$, the following decomposition $\mathbb{A}_E = UDV^H$ with U and V a set of orthonormal vectors and D a diagonal matrix. The amplitude distribution $A_{E\ ef\ m}$ and the functions $\lambda_{E\ ef\ m}$ are given by the M columns of UD and the M lines of V^H associated to the highest singular values of D .

In order to obtain a means of comparison for the study of reducibility, we also construct a more classical low rank approximation of the solution. Thus the pressure field $p(x, \omega)$ is also approximated as $\approx \tilde{p}^M = \sum_{m=1}^M \phi_m(\mathbf{x}) f_m(\omega)$ using a SVD. Such a decomposition is efficient for the low frequency range. It has been extended to the mid-frequency range, for example in the Padé approach [22], but the efficiency of this approach remains limited when the modal density is high.

The example concerns, once again, a quadrangular geometry and a frequency range $I_\omega: [\omega_0 - \Delta\omega, \omega_0 + \Delta\omega]$ with $\omega_0 = 2\pi.2500$ and $\Delta\omega = \alpha\omega_0$ for various values of α ranging between 5% and 30%. This means that, for 30%, the frequency bandwidth which is considered is [1750, 3250] Hz. The energy response is illustrated in Fig. 8 for a bandwidth of 10%.

The reference solution is built with the VTCR method with one VTCR element and 127 rays. One can notice that the response of the structure strongly depends on the level of damping.

In order to estimate whether the problem could be reduced efficiently, we look at the number of modes necessary to obtain the error ϵ_{I_ω} (Eq. (29)) less than 5%. In addition we compare the solution associated to the reduced the effective amplitude distribution to the reduced pressure field decomposition.

$$\epsilon_{I_\omega}^2(p^M) = \frac{\int_{I_\omega} \sum_{E=1}^{N_\Omega} \|p_{ref} - p_E^M\|_{S_E}^2 d\omega}{\int_{I_\omega} \sum_{E=1}^{N_\Omega} \|p_{ref}\|_{S_E}^2 d\omega} \tag{29}$$

In Fig. 9 the number of modes in function of the damping η and in function of the band width $\Delta\omega$ at the bottom, at the right for the quadrilateral are presented.

We observe from Fig. 9 (a) and (b) that the decomposition using the effective portrait performs better than the one based on the solution, especially for large bandwidths. The main remark, which will be exploited later is the strong influence of the damping. For example for a $\eta = 10^{-2}$, less than 15 modes of the effective portrait are sufficient in order to represent accurately the solution over the frequency domain [1750, 3250] Hz. On the contrary, for very small damping coefficients, a large number of modes is needed.

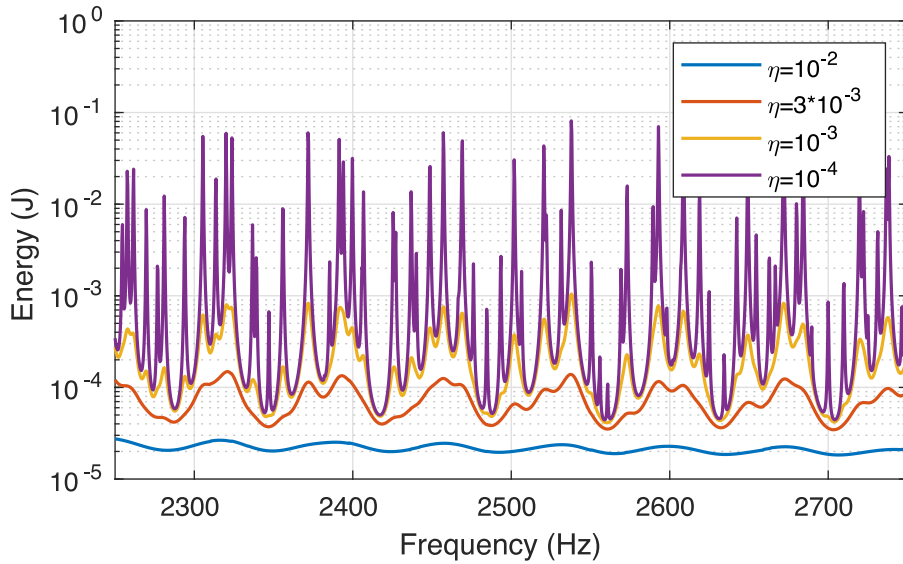


Fig. 8. Energy in the acoustic cavity as a function of frequency for different damping.

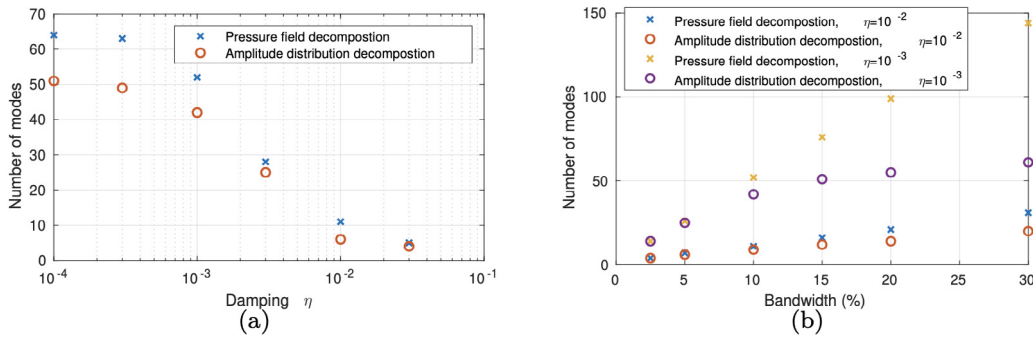


Fig. 9. Number of modes required for an error less than 5% for the pressure and for the effective amplitude distribution: (a) in function of the damping, (b) in function of the bandwidth for $\eta = 10^{-2}$ and $\eta = 10^{-3}$.

6. A priori reduction using the PGD method

In the previous part we studied the reducibility by constructing a low rank approximation of the solution knowing it. The challenge is to be able to compute directly, that is without knowing the solution, a reduced approximation of the solution which could lead to cost savings. Here, the reduced solution obtained using the SVD in the previous paragraph serves as reference.

6.1. Principle and method

The a priori reduction method called Proper Generalised Decomposition (in short PGD) [28] is used to search directly a low rank approximation of the solution. An approximate solution $A^M(\omega)$ of the VTCR problem is sought as:

$$A^M(\omega) = \sum_{m=1}^M \lambda_m(\omega) A_m \tag{30}$$

Once again A_m is a vector which contains a contribution to the portrait of all the elements. The associated modulation $\lambda_m(\omega)$ is a scalar function. The best decomposition is sought through the minimisation of a norm over I_ω of the

following residue:

$$R^M(\omega) = K(\omega)A^M(\omega) - F(\omega) \quad (31)$$

Different choice of the norm can be made. Considering the properties of the operator $K(\omega)$ (non-symmetrical and non-Hermitian matrix) we opt here for an L_2 norm.

$$\|R\|_2^2 = \int_{I_\omega} R^H R d\omega \quad (32)$$

A Petrov–Galerkin version of the PGD, as proposed in [29], would be probably more efficient but is technically more demanding. The best possible approximation using the L_2 norm is defined as:

$$A^M = \operatorname{argmin}(\|R^M(\omega)\|_2^2) \quad (33)$$

The direct resolution of the problem (33) is particularly expensive and does not allow for calculation savings. The classic approach to build the modes $(\Lambda_m, \lambda_m(\omega))$ is iterative and makes use of a greedy approach. In such an approach the couples $(\Lambda_m, \lambda_m(\omega))_{[1\dots M-1]}$ being assumed known, the couple $(\Lambda_M, \lambda_M(\omega))$ is determined such that:

$$(\Lambda_M, \lambda_M(\omega)) = \operatorname{argmin}(\|K(\omega)\lambda_M(\omega)\Lambda_M(\omega) - R^{M-1}(\omega)\|_2^2) \quad (34)$$

In order to have a problem with only one unknown, either Λ_M or $\lambda_M(\omega)$, the problem is solved iteratively. A uniform initialisation on the amplitude distribution is applied. This initialisation is denoted Λ_{M-0} . From it the best associated modulation $\lambda_{M-0}(\omega)$ is determined minimising the residue. From the value of $\lambda_{M-0}(\omega)$ the best possible associated value of Λ_{M-1} of the associated portrait is computed and so on. The process is stopped when two consecutive iterates are closed enough. Then, depending on the value of $\|R^M\|_2$, a new couple is added or the procedure is considered to be converged. In order to improve the convergence of this algorithm, different strategies are possible. In what follows we compare the results of the PGD obtained using 3 strategies:

- Strategy 1: the Greedy one described previously.
- Strategy 2: Strategy 1 + update of frequency functions previously determined after each new mode computation. This is the most classical approach for the PGD.
- Strategy 3: The strategy 2 is first applied to update the different modulations. From this new modulation, the different associated portrait is recomputed globally. Such a strategy is no more greedy.

The different strategies are illustrated for the quadrilateral at $\eta = 10^{-2}$ and $\eta = 10^{-3}$ over the frequency band I_ω defined by $\omega_0 = 2\pi.2500$ with $\Delta\omega = 10\% \omega_0$.

The case $\eta = 10^{-2}$, illustrated in Fig. 10, corresponds to a relative low modal density. The case $\eta = 10^{-3}$, illustrated in Fig. 11, corresponds to a much higher modal density.

It appears that the strategy 3 performs well with a ratio of modes around 1.5 compared to the SVD. This ratio tends to increase when seeking to very high precision.

From Figs. 10(a) and 11(b) it appears that, even for a quite important level of error, the quality of the reconstructed solution is quite satisfactory. This indicates that the error defined in Eq. (32) is severe. In fact this norm is sensitive to a small shift in frequency, which, in fact, has a low impact on the quality of the solution. This aspect should lead in the future to seek for better indication of the quality of low-rank approximation.

As for the SVD of the solution the number of mode needed for the PGD to approximate properly the solution is very sensitive to the damping coefficient. This is why we have sought for a computational strategy based on the exponential window method for which the calculations are performed with an artificial damping having a higher value than the real one.

7. The exponential window method applied to the VTCR

The exponential window method (EWM) was initially introduced in [25] to eliminate the free-vibration interval that appears in the standard DFT approach. It consists in searching for the Fourier transform of the time response multiplied by an exponential window. This method leads to the resolution of a frequency problem in which a damping is artificially added. Applying the EWM within in the context of the TVRC does not present difficulties. The main issue is elsewhere, the quality of the reconstructed solution is sensitive to the “damping parameter” of the method. To tune this parameter comparison between a resolution performed with VTCR in the classical frequency

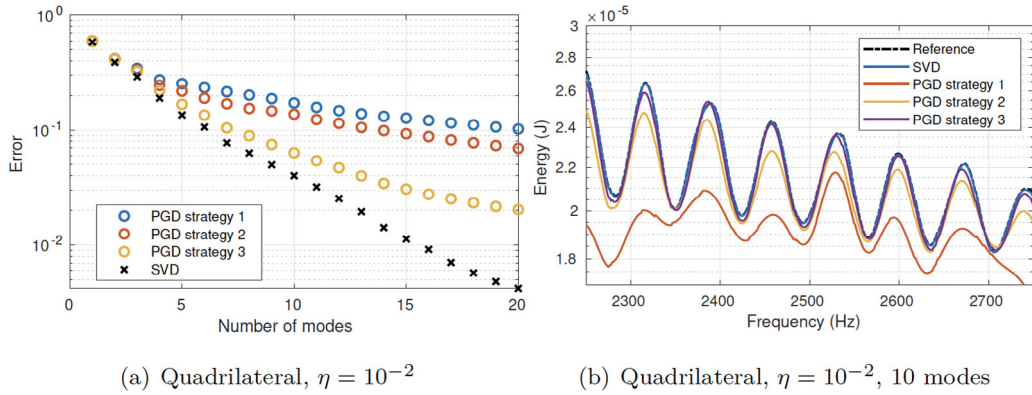


Fig. 10. Convergence of the different strategies for $\eta = 10^{-2}$: (a) error with respect to the number of mode (b) approximation of the energy of the cavity for ten modes.

domain and in the modified frequency domain are performed. The comparisons concern the reconstructed solution in the time domain. Here, the objective is to compute the transient response over a given period of time of the order of several wave round trips. It is therefore necessary to reconstruct the frequency content that contributes to the initial response only.

7.1. Development of the method

In the context of the paper the method may be summarised as follows. Rather than searching for the Fourier transform of the p field, the Fourier transform of the field $p_\alpha = e^{-\alpha t} p$ where $\alpha \in \mathbb{R}^+$ is searched.

$$P^\alpha(\omega) = TF(p_\alpha)(\omega) = TF(e^{-\alpha t} p)(\omega) = \int_{-\infty}^{\infty} p(t)e^{-i(\omega-i\alpha)t} dt = P(\omega - i\alpha) \quad (35)$$

Thus the problem to be solved in the frequency domain consists in solving the problem with modified inner and border equations. The problem (6) becomes: find, in each element E , the pressure field P_E^α such that:

$$\left\{ \begin{array}{l} \Delta P_E^\alpha + k_\alpha^2 P_E^\alpha = 0 \quad \text{in } \Omega_E \times I_\omega \\ z \frac{\partial P_E^\alpha}{\partial \mathbf{n}_E} + i(\omega - i\alpha)\rho P_E^\alpha = H_d^\alpha \quad \text{over } \partial_h \Omega_E \times I_\omega \\ P_E^\alpha = P_d^\alpha \quad \text{over } \partial_p \Omega_E \times I_\omega \\ -\frac{\partial P_E^\alpha}{\partial \mathbf{n}_E} = i(\omega - i\alpha)\rho V_d^\alpha \quad \text{over } \partial_v \Omega_E \times I_\omega \\ P_E^\alpha = P_{E'}^\alpha \quad \text{over } \Gamma_{E,E'} \times I_\omega \\ \frac{\partial P_E^\alpha}{\partial \mathbf{n}_E} = -\frac{\partial P_{E'}^\alpha}{\partial \mathbf{n}_{E'}} \quad \text{over } \Gamma_{E,E'} \times I_\omega \end{array} \right. \quad (36)$$

where:

$$k_\alpha = \frac{\omega - i\alpha}{c}(1 - i\eta) = \frac{\omega - \alpha\eta}{c} \left(1 - i \left(\frac{\eta + \alpha/\omega}{1 - \alpha\eta/\omega} \right) \right) \quad (37)$$

When comparing to the original formulation where:

$$k = \frac{\omega}{c}(1 - i\eta) \quad (38)$$

the method introduces a modified damping coefficient and a modified celerity as follows:

$$\begin{aligned} \eta_\alpha &= \frac{\eta + \alpha/\omega}{1 - \alpha\eta/\omega} \\ c_\alpha &= \frac{c}{1 - \alpha\eta/\omega} \end{aligned} \quad (39)$$

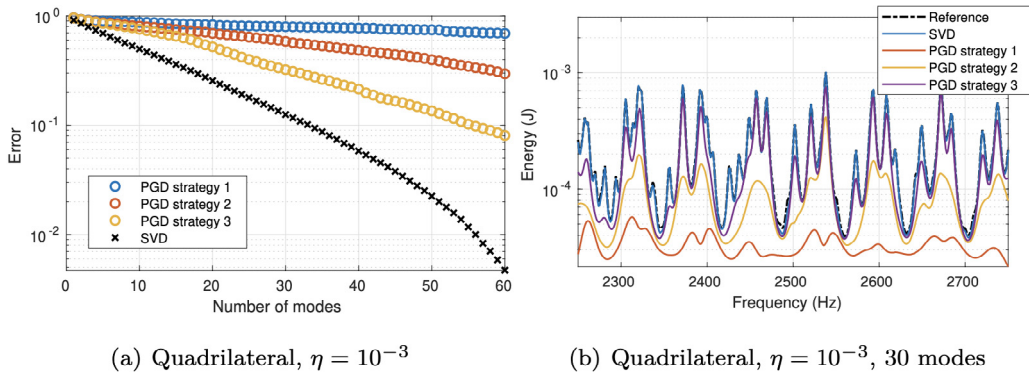


Fig. 11. Convergence of the different strategies for $\eta = 10^{-3}$: (a) error with respect to the number of mode (b) approximation of the energy of the cavity for thirty modes.

Solving this problem with the VTCT therefore consists in modifying the shape functions which become: $e^{ik_{\alpha}\mathbf{n}(\theta)\cdot(\mathbf{x}-\mathbf{x}_0)}$, and the modified Neumann and Robin border conditions defined by Eq. (36).

To recover the original solution from the modified frequency one applies the following inverse transform:

$$p(t) = e^{\alpha t} p_{\alpha}(t) = e^{\alpha t} T F^{-1}(P^{\alpha})(t) \tag{40}$$

In [25] the author has proposed and justified the use of the following value for α denoted α_r ,

$$\alpha_r = \frac{\ln(100)}{T} \approx \frac{4.6}{T} \tag{41}$$

This explains why the method is mostly adapted to transient analysis, the shorter T the larger α . Moreover, for this a choice, the frequency step can be taken as $\delta\omega \approx \frac{2\pi}{T}$ and is therefore much larger than the one used for the original formulation.

The resolution requires to multiply the time signals by the exponential window, then to apply the Fourier Transform and perform the calculations in the modified frequency domain with the VTCT (frequency by frequency) and, finally, to return to the time domain.

In order to validate this approach, a transient problem of a quadrilateral acoustic cavity is solved. The fluid is characterised by its celerity $c = 340 \text{ m s}^{-1}$ and its damping coefficient $\eta = 1.10^{-3}$. The edge conditions are zero Dirichlet conditions everywhere except on the left wall where the pressure is imposed as:

$$p_d(t, x) = \frac{1 - \cos(2\pi x)}{2} * e^{\frac{-(t-t_{depa.})^2}{\Delta t^2}} \cos(2\pi f_{cent.}t) \tag{42}$$

In Eq. (42) x is the curvilinear abscissa of the left edge. The following values are used: $t_{depa.} = 2.2 \text{ ms}$, $\Delta t = 0.59 \text{ ms}$ and $f_{cent.} = 2500 \text{ Hz}$. This signal has a frequency content centred on 2500 Hz and which expands between 1000 Hz and 4000 Hz as shown in Fig. 12.

The problem is studied over a time range $I_T = [0; 6\frac{L}{c}] = [0; 23] \text{ ms}$, with L the characteristic cavity dimension. Several values of α have been tested around the proposal of Hall [25]: $\frac{\alpha}{4} = 50 \text{ rad s}^{-1}$, $\alpha_r = 200 \text{ rad s}^{-1}$ and $4\alpha_r = 800 \text{ rad s}^{-1}$. The energy in the modified frequency domain is shown in Fig. 13. We clearly see the influence of α on the apparent damping.

In Fig. 14 the reference value of the pressure in a representative point of the cavity is presented at the top. The difference between the reference and the obtained value of the pressure is presented at the bottom as a function of α .

As expected, there is an almost perfect superposition of the different temporal responses of the signal for $\alpha = 50 \text{ rad s}^{-1}$ and $\alpha = 200 \text{ rad s}^{-1}$. For $\alpha = 800 \text{ rad s}^{-1}$ the difference with the reference diverges exponentially. This allows to understand the compromise that has to be done for the method to work. One wishes to chose α as large as possible. Nevertheless, for α too large, the multiplication by $e^{\alpha t}$ in the inverse transform (Eq. (40)) renders the method unstable. A numerical study was conducted in order to determine the value of α , denoted by α_{lim} for which the solution starts to diverge. Due to the relation between T and α , the results may also be interpreted as the value

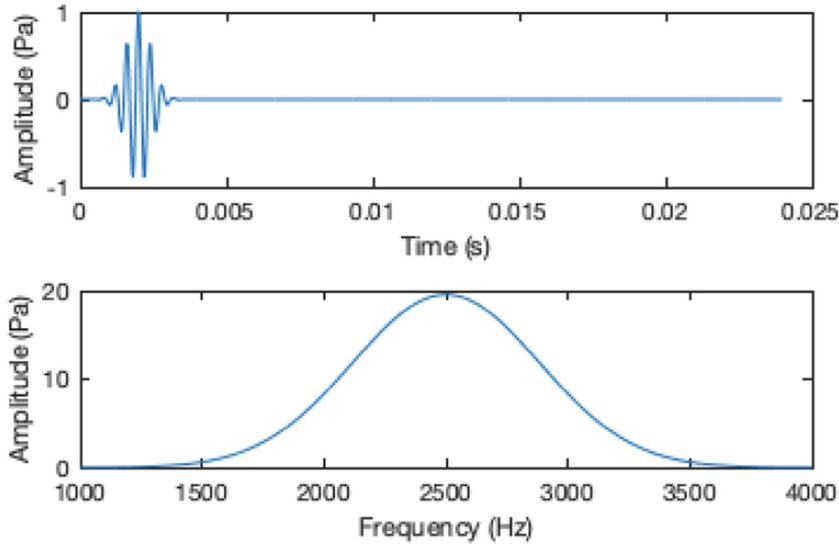


Fig. 12. Input signal p_d in time domain (top) and frequency domain (bottom).

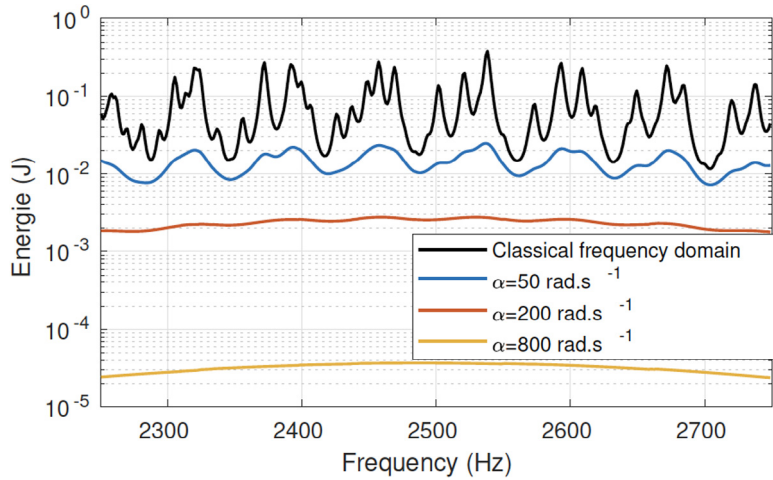


Fig. 13. Energy of the solution in the modified frequency domain for different values of the α parameter.

of T_{lim} of T for which the solution starts to diverge. The results are presented Fig. 15. For both cases we obtain the heuristic relation:

$$\alpha_{lim} \approx \frac{9.5}{T_{lim}} \approx 2\alpha_r \tag{43}$$

As can be seen in Fig. 15 two discretisation steps have been used. The first one corresponding to $\delta\omega \approx \frac{2\pi}{T}$ and the other is about four times finer. In this range of values, the discretisation steps do not seem to play a role regarding the instability.

8. Coupling of the VTCR wide frequency band resolution method and the exponential window method

8.1. Preliminary remarks on the applicability of the approach

In this section the PGD model reduction method is applied to the VTCR in the modified frequency domain. The objective is to construct, at a lower cost, an approximation of the transient response in the time domain. Rather

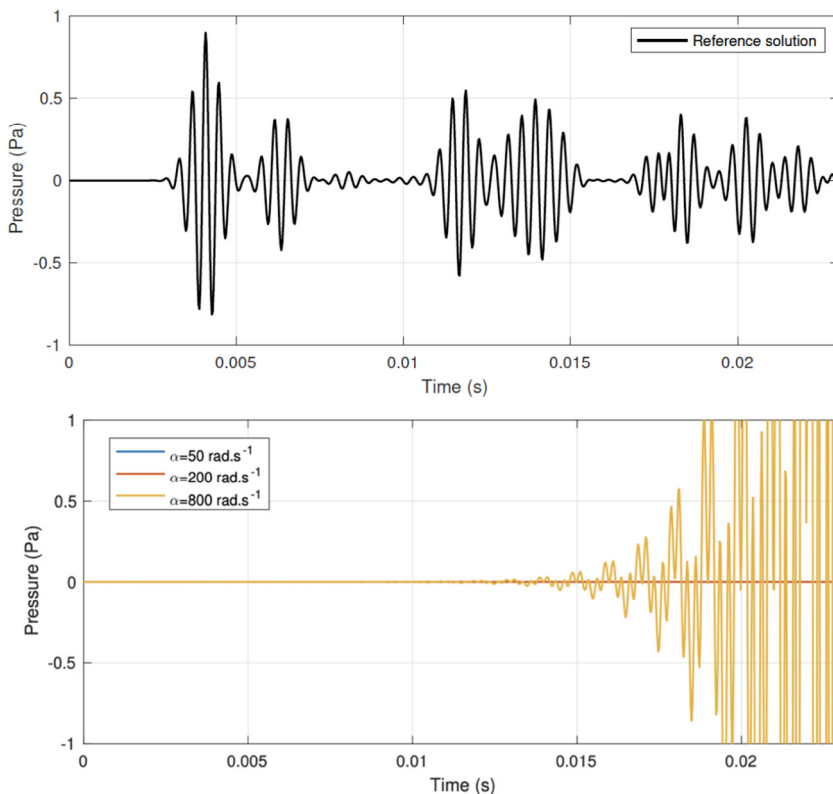


Fig. 14. Top: classical frequency resolution approach, bottom: difference between the reference and the coupled VTCR-exponential window approach.

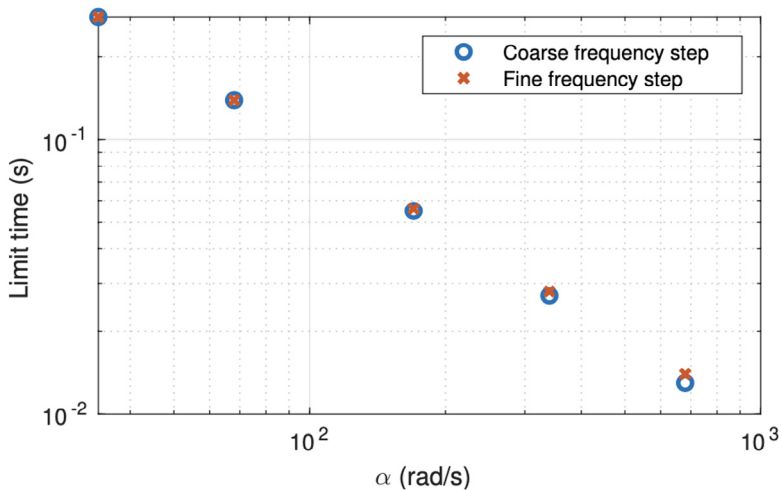


Fig. 15. Relation between T_{lim} and α_{lim} .

than solving the modified frequency problem frequency by frequency, like presented in Section 7, the PGD large band resolution method is applied. The approach is expected to benefit from the fact that the exponential window method leads to the resolution of a highly damped problem in the frequency domain. This is a range of problems in which the PGD model reduction applied to the VTCR is effective. The previous paragraph allows trying to a

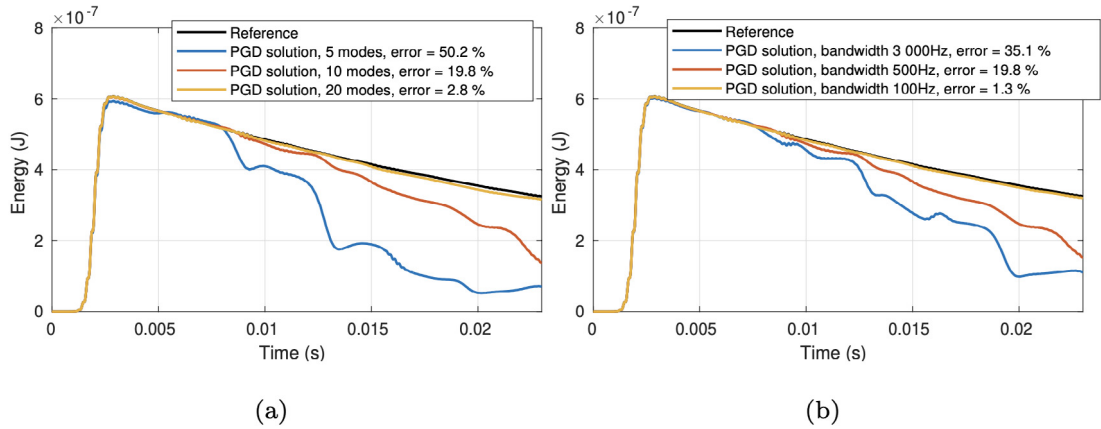


Fig. 16. Energies of the different solution: the reference and the PGD solution. (a): solution with respect to the number of modes for a frequency band of 500 Hz. (b): solution with respect to the bandwidth for 10 modes.

priori tune the method. In fact, it is expected that the PGD would lead to a precise solution using between 5 modes ($\eta = 10^{-2}$) up to 20 modes ($\eta = 5 \cdot 10^{-2}$). Moreover, choosing α of the order of α_r we have, for $\eta = 10^{-3}$ and T of the order of a tenth of millisecond 10 ms, and for a frequency of the order of 2000, the following valuable approximation of η_α is obtained.

$$\eta_\alpha = \frac{\eta + \alpha/\omega}{1 - \alpha\eta/\omega} \approx \alpha/\omega \approx \frac{1}{fT} \tag{44}$$

Leading to the following estimate of η_α over the frequency band $[f_{min}, f_{max}]$:

$$\eta_\alpha \in \left[\frac{1}{f_{max}T}, \frac{1}{f_{min}T} \right] \tag{45}$$

For the previous example one therefore has $\eta_\alpha \in [10^{-2}, 4 \cdot 10^{-2}]$ a range for which the PGD reduction is, a priori, interesting. Moreover, due to the Parseval relationship, the quality of the reconstruction is expected to decrease with the time. Indeed:

$$\int_{t=-\infty}^{\infty} |f|^2 dt = \int_{\omega=-\infty}^{\infty} |F|^2 d\omega \tag{46}$$

where F is the Fourier transform of f . In the modified frequency domain this becomes:

$$\int_{-\infty}^{\infty} |f|^2 e^{-2\alpha t} dt = \int_{-\infty}^{\infty} |F_\alpha|^2 d\omega \tag{47}$$

Thus the larger α , the more the PGD algorithm will privilege short times.

8.2. First example

We consider once again the case studied in Section 7. The PGD broadband resolution method is applied on frequency bands with a width of $\Delta\omega = 500$ Hz. In Fig. 16 the mechanical energy $\|\cdot\|_E^2$ in function of the time for the reference solution and the PGD approximation are presented. The results have been obtained using a value of $\alpha = 170$ rad/s a little bit smaller than $\alpha_r = 200$ rad/s. The idea is to potentially compensate for the additional error induced by the PGD approximation.

These results are in agreement with what was expected and commented in Section 8.1. This gives us confidence that the method could be well mastered and automatized in the near future. Let us consider the first instance, that the computational costs are proportional to the total number of modes M (sum of modes over all frequency bands). It appears, from the previous figures, that the most interesting strategy is to take wide frequency bandwidths.

In order to quantify the gains brought by the coupling, the transient response using the PGD without the artificial damping on 500 Hz frequency bands has been applied. In this case 80 modes were needed to reconstruct the

transient response with an error of about 5%. This is about 5 times more modes than when $\alpha = 170 \text{ rad s}^{-1}$. In Fig. 17, the reconstructed solution with only ten modes is plotted (with 20 modes it is not possible to see any differences). Once again one notice that the error is concentrated at the last instant. Once again the measure of error, in this case 19.8% seems quite severe with respect to the quality of the reconstructed field.

9. PGD-VTCR applied to a shock propagation in an acoustic cavity over a long period of time

We consider here a problem mimicking a shock on an acoustic cavity illustrated in Fig. 18.

The example involves two challenges. First, to properly evaluate the energy of the response, one has to consider a large frequency content (up to 15 KHz). Moreover the solution is searched over a long period of time involving about 10 return trips, i.e. 200 ms. This example will serve both to illustrate the method but also to understand the difficulties we will have to take into account in future applications.

The damping is $\eta = 0.001$. The cavity is loaded by a triangular short time signal as shown in Fig. 19, imposed as a Dirichlet condition, see Fig. 18.

9.1. A first attempt to apply the method for a long period of time and a large frequency spectrum

The first aspect is to separate the low and high frequency contributions such as described in [26]: the low frequencies are considered belonging to $[0, 900]$ Hz. To deal with the low frequencies a modal base considering all modes with an eigenfrequency up to 1800 Hz is used. The high-frequency part is solved using the large-band VTCR PGD resolution coupled with the exponential window method. For the duration considered 200 ms and for α close to α_r , the value of η_{α} would be around $2 \cdot 10^{-3}$. Obtaining a precise solution with such a low value would be very costly, leading either using a lot of modes or dealing with very small bandwidths.

Yet a precise estimation of the solution in the first instant after the shock is very important. Moreover the times going on the solution becomes more and more diffuse and not deterministic. Numerically this reflects in the fact that it is nearly impossible to achieve a precise solution due to the phase shift. To compare the temporal response over such a long period of time is neither meaningful nor interesting. This is why a common practice, especially in industry, is to characterise the long term response by its hock Response Spectrums (SRS). The SRS corresponds to the maximum in acceleration of the response of a single degree of freedom system with quality factor Q subjected to the signal in function of the natural frequency of that system. To address the previous issue the time domain is divided into two subdomains. The first one, $[0, 25]$ ms], where one wishes to compute quite accurately the solution. For the second one $[25, 200]$ ms] for which a correct approximation of the SRS is looked for.

9.1.1. The transient response on a short time

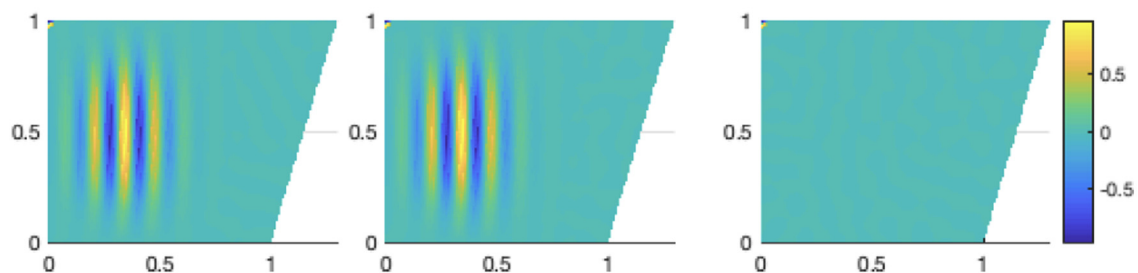
As the response must be reconstructed on a duration of 0.025 s, $\alpha = 160 \text{ rad s}^{-1} \approx 4/T$ is chosen. As the PGD is efficient for important damping, wide frequency bands are used, of the order of 30%. Moreover the computation make use, a priori, of 20 modes. To simplify the resolution we will take regular size bands: 13 bands of 1185 Hz, which corresponds about to a 30% bandwidth at 2000 Hz. The response is shown in Fig. 20 at points 1, 2 and 3. The answer near the source (at point 1) shows the arrival of the wave in the cavity at the instant $t = 1.05$ ms. This portion of the signal is similar to the source signal, which makes it possible to validate the reconstruction of the response. The error in L2 norm with respect to the reference is 2.24%, 13.9% and 16.1% at nodes 1, 2 and 3 respectively. The reference is reconstructed from a point-to-point frequency resolution.

In order to obtain a better solution we should adapt the number of mode or the bandwidth depending on the frequency. In fact if $\eta_{\alpha} \approx 0.02$ at 2000 Hz it is only of the order of $\eta_{\alpha} \approx 0.005$ at 10 000 Hz. Hence the use of 20 modes is not sufficient for the high part of the spectrum where one should probably use around 40 modes.

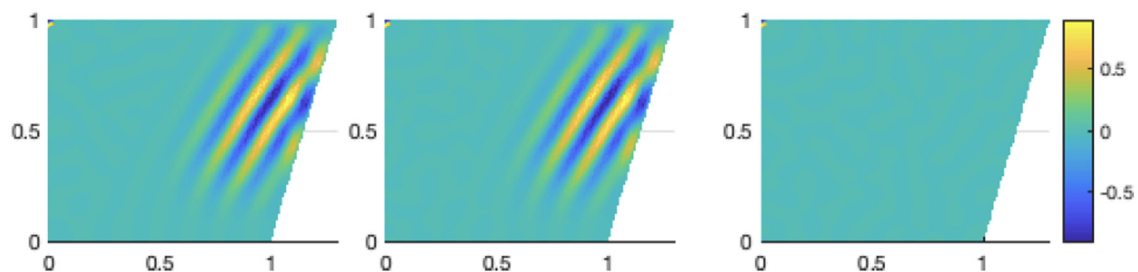
9.1.2. The transient response on a long time

As we consider a much larger value of T, this induces much lower artificial damping than before $\eta_{\alpha} \approx 0.0026$ at 2000 Hz. Since the PGD reduction is less efficient on this damping range, bandwidths of around 5% are chosen. This leads to introduce 80 regular bands of 192 Hz. Once again the solution is approximated using 20 modes per band.

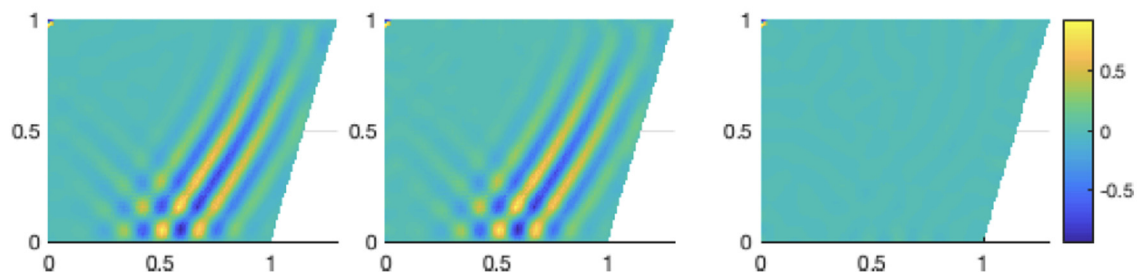
The SRS of the reduced model approach and of the reference are constructed and represented Fig. 21 with quality factor $Q = 10$. SRS curves have a classic appearance. They are asymptotically divided into two parts: a



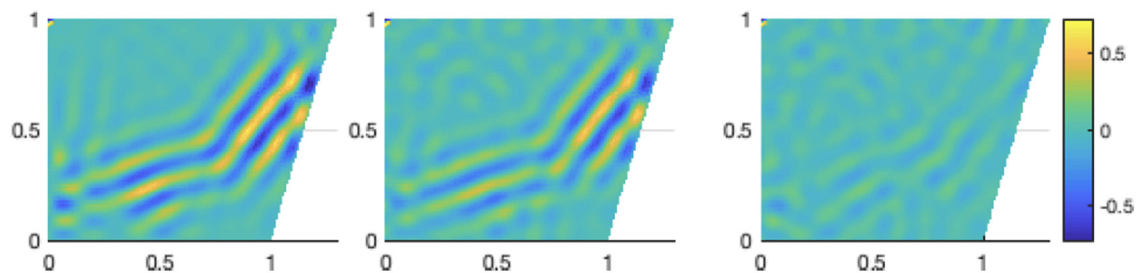
(a) $t = 3ms$



(b) $t = 6ms$



(c) $t = 12ms$



(d) $t = 20ms$

Fig. 17. Pressure fields in time domain at different time steps. At the left, the reference fields, at the middle, the PGD fields (10 modes, $\alpha = 170 \text{ rad s}^{-1}$ and frequency band of 500 Hz), at the right the difference between the two fields.

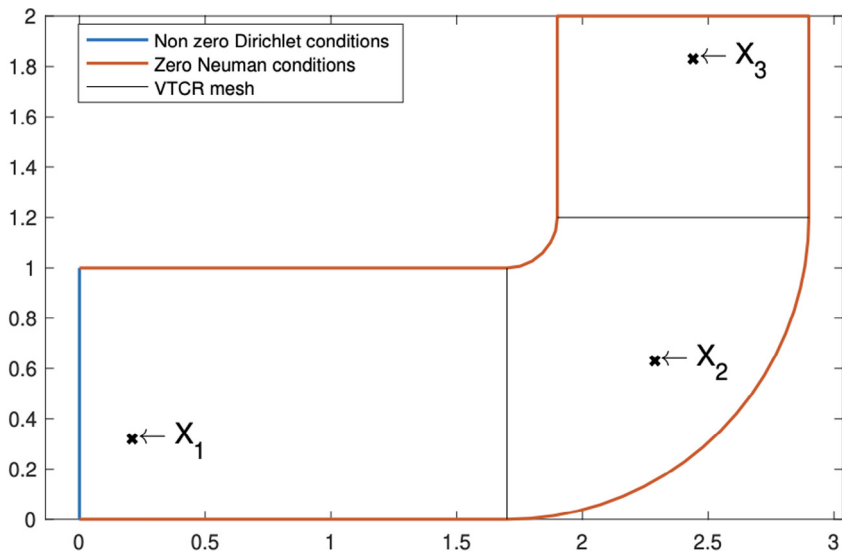


Fig. 18. Acoustic cavity (length in m) submitted to the shock.

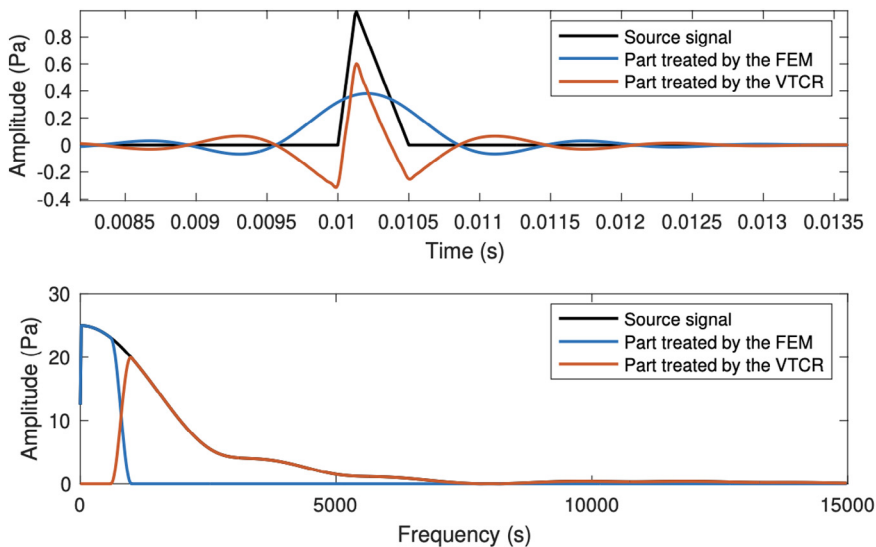


Fig. 19. Shock signal decomposed into a low-frequency part and a high-frequency part.

20db/decade slope and a plateau. Moreover, one notices some reasoning due to certain excited eigenmodes. Let us compare the SRS from the reduced model approach with those from the reference. At point X_1 (left) we notice a very good agreement between the model reduction approach and the reference in low frequency and high frequency. At point X_3 differences are present around 1000 Hz, the answer is slightly underestimated by the reduced model.

Conclusion

In this paper a model reduction strategy in the frequency domain for the reconstruction of the transient response of dynamics problems has been proposed. The concept of effective portraits has allowed to improve the efficiency of the reduced approach. The reducibility of the problem in function of the frequency bandwidth and of the damping has been studied. A key point is that the greater the damping, the more reducible the problem is. This leads to introducing the exponential window method (EMW), which allows to artificially add a configurable damping. The

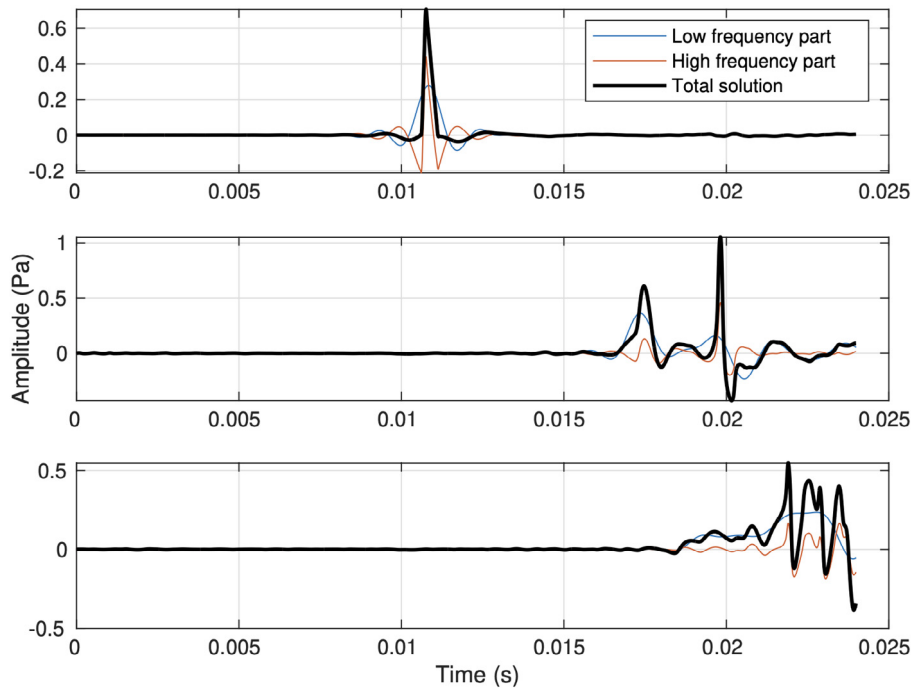


Fig. 20. Time response at points X_1 , X_2 and X_3 (respectively from top to bottom) of the 18 cavity computed with the reduced model approach.

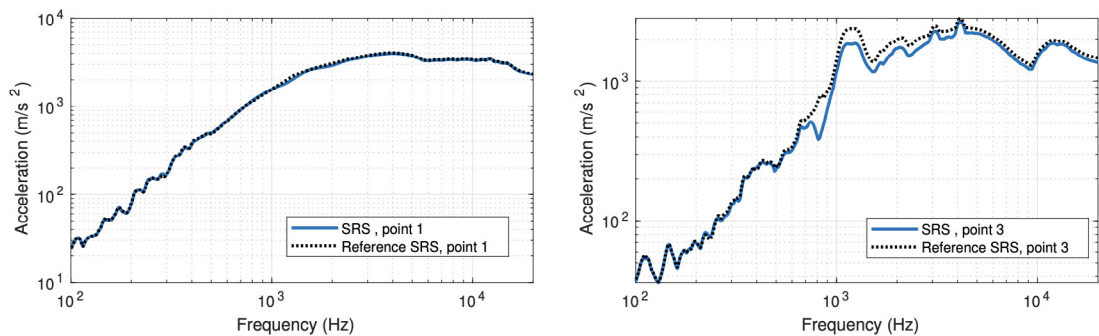


Fig. 21. SRS (quality factor of the SRS $Q = 10$) at point X_1 (left) and point X_3 (right) of the 18 cavity built from a resolution over a long period of time.

coupling of the EMW and the TVRC has allowed studying the influence of the artificial damping parameters. The whole study has allowed mastering the coupling between the PGD-VTCR broadband resolution and the EMW. Illustrations concerning the approximation of the transient response of a dynamic problem has been proposed. In particular it has allowed to deal with the response of a simple 2D acoustic cavity to a shock problem including a large frequency content and over a long period of time. The efficiency of the method is still to be assessed on more representative examples and will probably lead to optimised the different steps of the approach with respect to their costs.

Declaration of competing interest

The authors declare that they have no known competing financial interests or personal relationships that could have appeared to influence the work reported in this paper.

References

- [1] O. Zienkiewicz, *The Finite Element Method Volume 1: The Basis*, Butterworth-Heinemann, 2000.
- [2] A. Deraemaeker, I. Babuška, P. Bouillard, Dispersion and pollution of the FEM solution for the Helmholtz equation in one, two and three dimensions, *Internat. J. Numer. Methods Engrg.* 46 (1999) 471–499, [http://dx.doi.org/10.1002/\(SICI\)1097-0207\(19991010\)46:4<471::AID-NME684>3.0.CO;2-6](http://dx.doi.org/10.1002/(SICI)1097-0207(19991010)46:4<471::AID-NME684>3.0.CO;2-6).
- [3] F. Ihlenburg, B. IM, Finite element solution of the Helmholtz equation with high wave number part I: The h-version of the FEM, *Comput. Math. Appl.* 30 (1995) 9–37, [http://dx.doi.org/10.1016/0898-1221\(95\)00144-N](http://dx.doi.org/10.1016/0898-1221(95)00144-N).
- [4] I. Harari, T. Hughes, Galerkin/least-squares finite element methods for the reduced wave equation with non-reflecting boundary conditions in unbounded domains, *Comput. Methods Appl. Mech. Engrg.* 98 (1992) 411–454, [http://dx.doi.org/10.1016/0045-7825\(92\)90006-6](http://dx.doi.org/10.1016/0045-7825(92)90006-6).
- [5] C. Soize, Reduced models in the medium frequency range for general dissipative structural-dynamics systems, *Eur. J. Mech. A Solids* 17 (1998) 657–685, [http://dx.doi.org/10.1016/S0997-7538\(99\)80027-8](http://dx.doi.org/10.1016/S0997-7538(99)80027-8).
- [6] J. Melenk, I. Babuška, The partition of unity finite element method: Basic theory and applications, *Comput. Methods Appl. Mech. Engrg.* 139 (1996) 289–314, [http://dx.doi.org/10.1016/S0045-7825\(96\)01087-0](http://dx.doi.org/10.1016/S0045-7825(96)01087-0).
- [7] T. Strouboulis, R. Hidajat, Partition of unity method for Helmholtz equation: Q-convergence for plane-wave and wave-band local bases, *Appl. Math.* 51 (2006) 181–204, <http://dx.doi.org/10.1007/s10492-006-0011-0>.
- [8] J. Zitelli, I. Muga, L. Demkowicz, J. Gopalakrishnan, D. Pardo, V. Calo, A class of discontinuous Petrov–Galerkin methods. Part IV: The optimal test norm and time-harmonic wave propagation in 1D, *J. Comput. Phys.* 230 (2011) 2406–2432, <http://dx.doi.org/10.1016/j.jcp.2010.12.001>.
- [9] P. Ladèveze, A new computational approach for structure vibrations in the medium frequency range, *Comptes Rendus de L'Académie Des Sci. Série II Fascicule B-Mécanique Phys. Chime Astronomie* 322 (1996) 849–856.
- [10] W. Desmet, B. van Hal, P. Sas, D. Vandepitte, A computationally efficient prediction technique for the steady-state dynamic analysis of coupled vibro-acoustic systems, *Adv. Eng. Softw.* 33 (7) (2002) 527–540, [http://dx.doi.org/10.1016/S0965-9978\(02\)00062-5](http://dx.doi.org/10.1016/S0965-9978(02)00062-5), Engineering Computational Technology & Computational Structures Technology.
- [11] C. Farhat, I. Harari, U. Hetmaniuk, The discontinuous enrichment method, *Comput. Methods Appl. Mech. Engrg.* 192 (2003) 3195–3209, [http://dx.doi.org/10.1016/S0045-7825\(03\)00344-X](http://dx.doi.org/10.1016/S0045-7825(03)00344-X).
- [12] E. Perrey-Debain, J. Trevelyan, P. Bettess, Plane wave interpolation in direct collocation boundary element method for radiation and wave scattering: Numerical aspects and applications, *J. Sound Vib.* 261 (2003) 839–858, [http://dx.doi.org/10.1016/S0022-460X\(02\)01006-4](http://dx.doi.org/10.1016/S0022-460X(02)01006-4).
- [13] B. W. Desmet, O. Atak, "Mid-Frequency", *CAE Methodologies for Mid Frequency Analysis in Vibration and Acoustics*, Katholieke Universiteit Leuven, Faculty of engineering Heverlee Belgium, 2012.
- [14] R. Hiptmair, A. Moiola, I. Perugia, A survey of trefftz methods for the Helmholtz equation, *Building Bridges: Connections and Challenges in Modern Approaches to Numerical Partial Differential Equations*, 2015.
- [15] P. Ladèveze, L. Arnaud, P. Rouch, C. Blanzé, The variational theory of complex rays for the calculation of medium-frequency vibrations, *Eng. Comput.* 18 (2001) 193–214, <http://dx.doi.org/10.1108/02644400110365879>.
- [16] A. Cattabiani, H. Riou, A. Barbarulo, P. Ladèveze, G. Bezier, B. Troclet, The variational theory of complex rays applied to the shallow shell theory, *Comput. Struct.* 158 (2015) <http://dx.doi.org/10.1016/j.compstruc.2015.05.021>.
- [17] H. Riou, P. Ladèveze, B. Sourcis, The multiscale VTCR approach applied to acoustics problems, *J. Comput. Acoust.* 16 (2008) 487–505, <http://dx.doi.org/10.1142/S0218396X08003750>.
- [18] P. Ladèveze, M. Chevreuril, A new computational method for transient dynamics including the low- and the medium-frequency ranges, *Internat. J. Numer. Methods Engrg.* 64 (4) (2005) 503–527, <http://dx.doi.org/10.1002/nme.1379>, arXiv:<https://onlinelibrary.wiley.com/doi/pdf/10.1002/nme.1379>.
- [19] C. Rouzaud, F. Gatuingt, G. Hervé, O. Dorival, A new multi-frequency approach based on padé approximants for the treatment of transient dynamics problems with the variational theory of complex rays, *J. Sound Vib.* 392 (2017) 170–186, <http://dx.doi.org/10.1016/j.jsv.2016.12.026>.
- [20] L. Kovalevsky, P. Ladèveze, H. Riou, The Fourier version of the variational theory of complex rays for medium-frequency acoustics, *Comput. Methods Appl. Mech. Engrg.* 225 (2012) 142–153, <http://dx.doi.org/10.1016/j.cma.2012.03.009>.
- [21] L. Kovalevsky, P. Gosselet, A quasi-optimal coarse problem and an augmented Krylov solver for the variational theory of complex rays, *Internat. J. Numer. Methods Engrg.* 107 (2015) n/a–n/a, <http://dx.doi.org/10.1002/nme.5190>.
- [22] R. Djellouli, C. Farhat, R. Tezaur, A fast method for solving acoustic scattering problems in frequency bands, *J. Comput. Phys.* 168 (2001) 412–432, <http://dx.doi.org/10.1006/jcph.2001.6707>.
- [23] R. Rumpfer, P. Goransson, J.-F. Deü, A finite element approach combining a reduced-order system, padé approximants, and an adaptive frequency windowing for fast multi-frequency solution of poro-acoustic problems, *Internat. J. Numer. Methods Engrg.* 97 (2014) 759–784.
- [24] A. Barbarulo, P. Ladèveze, H. Riou, L. Kovalevsky, Proper generalized decomposition applied to linear acoustic: A new tool for broad band calculation, *J. Sound Vib.* 333 (11) (2014) 2422–2431, <http://dx.doi.org/10.1016/j.jsv.2014.01.014>.
- [25] J. Hall, J. Beck, Linear system response by DFT: Analysis of a recent modified method, *Earthq. Eng. Struct. Dyn. - Earthq. Eng. Struct. Dyn.* 22 (1993) 599–615, <http://dx.doi.org/10.1002/eqe.4290220705>.
- [26] M. Chevreuril, P. Ladèveze, P. Rouch, Transient analysis including the low- and the medium-frequency ranges of engineering structures, *Comput. Struct.* 85 (2007) 1431–1444, <http://dx.doi.org/10.1016/j.compstruc.2006.08.091>.
- [27] L. Kovalevsky, P. Ladèveze, H. Riou, M. Bonnet, The variational theory of complex rays for three-dimensional Helmholtz problems, *J. Comput. Acoust.* 20 (2012) <http://dx.doi.org/10.1142/S0218396X1250021X>.

- [28] F. Chinesta, P. Ladevèze, E. Cueto, A short review on model order reduction based on proper generalized decomposition, *Arch. Comput. Methods Eng.* 18 (2011) 395–404, <http://dx.doi.org/10.1007/s11831-011-9064-7>.
- [29] A. Nouy, A priori model reduction through proper generalized decomposition for solving time-dependent PDEs, *Comput. Methods Appl. Mech. Engrg.* 199 (2010) 1603–1626, <http://dx.doi.org/10.1016/j.cma.2010.01.009>.